Geosciences Journal
Vol. 11, No. 3, p. 211 − 217, September 2007

Full-waveform inversion algorithm for interpreting crosshole radar data: a theoretical approach

Seiichiro Kuroda, Mutsuo Takeuchi — *National Institute for Rural Engineering, 2-1-6 Kannondai, Tsukuba, Ibaraki 305-8609, Japan*
Hee Joon Kim* — *Pukyong National University, Busan 608-737, Korea*

ABSTRACT: Ground-penetrating radar is a useful tool for civil and environmental engineering fields because of its high resolving power and non-destructive measurements. This paper presents a method of full-waveform inversion of borehole radar data for imaging permittivity structures. The inversion algorithm is based on a conjugate gradient search for the minimum of an error functional relating to the difference between measured and predicted data. A small model perturbation in the functional can be efficiently calculated by propagating the data error back into the model in reverse time and correlating the field generated by the back-propagation with the corresponding incident field at each point. A finite difference time domain (FDTD) method is used for solving Maxwell's equations to obtain incident electromagnetic wavefields. Back-propagated wavefields satisfy adjoint Maxwell's equations, which are stable in reverse time and can be solved by the same FDTD scheme. The imaging scheme is applied to crosshole radar configuration, thereby demonstrating its capability to reconstruct permittivity structures. Tests on a two-dimensional synthetic model produce good images of target scatterers and show stable convergence.

Key words: radar, full-waveform inversion, conjugate gradient, permittivity, FDTD

1. INTRODUCTION

Many electromagnetic (EM) interpretations are now made in time domain because the recent progress of EM devices makes it possible to acquire EM data as a time series with a small sampling interval. Typical methods in time domain are time-domain EM (TEM), time-domain induced polarization, and ground-penetrating radar (GPR). Among these, the applicability and application area of the GPR method are rapidly expanded because of its easy use, quick operation, and high resolving power. However, it cannot be used for deeper sensing due to the strong attenuation of EM wave. Borehole radars are generally used in surveys for such deep targets, and employ the wave that propagates directly from source to receiver.

In crosshole seismic, typical approaches involve ray tomography and Fresnel volume tomography. Traveltime tomographies using ray tracing require high-frequency approximation, with maximum resolution on the order of a wavelength. Because of poor resolution, however, the usefulness of ray tomography may be limited if the objective is to better understand the petrophysical and hydrological properties of soils and rocks. An alternative to traveltime tomography is full-waveform inversion (Tarantola, 1984), which can improve resolution of velocity structures.

Wang et al. (1994) presented an imaging algorithm to produce interwell conductivity distribution from TEM data. Their imaging was based on a method of full-waveform inversion, which is first developed for seismic wavefields by Tarantola (1984). Newman and Commer (2005) extended the Wang et al's (1994) algorithm to formulate a three-dimensional TEM imaging scheme. Sanada et al. (1999a) also applied the Wang et al's (1994) algorithm to crosshole radar tomography to obtain conductivity distribution. In contrast, Jia et al. (2002) developed an inverse scattering method for imaging buried objects by crosshole radar. Their approach is quite efficient because of the restriction of unknowns to be a few variables instead of reconstructing unknown functions. Recently, Ha et al. (2004) inverted dc resistivity data by using an algorithm of reverse time migration, which can theoretically be tied with a single operation of nonlinear inversion by a gradient search (Tarantola, 1984).

In this paper we present an imaging algorithm for interpreting borehole radar data by applying the full-waveform inversion to EM wavefields. We try to solve this radar imaging as a standard problem of nonlinear optimization. The goal is to find a model that minimizes the data error, which is the norm of the difference between modeled and measured data. For this end a weighted sum-of-squares of L2 norm is used. An analysis shows that the gradient of the data error with respect to small changes in medium parameters about a given model can be computed efficiently by propagating the difference between actual and simulated data back into the model in reverse time and correlating the EM field obtained by this back-propagation with the incident field. This leads naturally to a conjugate gradient (CG) search for the best model. Each iteration requires only two forward simulations: one to compute the data in the current model, one to compute the gradient. In addition, several forward calculations are required to evaluate a step length

*Corresponding author: hejkim@pknu.ac.kr

along the CG direction. The inversion algorithm is verified using a synthetic model having non-uniform permittivity distribution.

2. GRADIENT OF ERROR FUNCTIONAL

The first-order Maxwell's equations with both electric and magnetic sources, **j** and **m**, are given by

$$\left(\varepsilon\frac{\partial}{\partial t}+\sigma\right)\mathbf{e}-\nabla\times\mathbf{h} = -\mathbf{j} \tag{1}$$

$$\nabla\times\mathbf{e}+\mu\frac{\partial\mathbf{h}}{\partial t} = -\mathbf{m} \tag{2}$$

where **e** and **h** denote electric and magnetic fields, respectively, ε permittivity, σ electric conductivity, and μ magnetic permeability. Solutions of the Maxwell's equations can be formally written using dyadic Green functions, $\mathbf{g}_{ij}$ (i, j = 1, 2; see Appendix A), as (Tai, 1993; Wang et al., 1994).

$$\mathbf{e}(\mathbf{r},t) = \int_{V,t}\mathbf{g}_{11}(\mathbf{r},t|\mathbf{r}',t')\cdot\mathbf{j}(\mathbf{r}',t')d\mathbf{r}'dt' + \int_{V,t}\mathbf{g}_{12}(\mathbf{r},t|\mathbf{r}',t')\cdot\mathbf{m}(\mathbf{r}',t')d\mathbf{r}'dt' \tag{3}$$

$$\mathbf{h}(\mathbf{r},t) = \int_{V,t}\mathbf{g}_{21}(\mathbf{r},t|\mathbf{r}',t')\cdot\mathbf{j}(\mathbf{r}',t')d\mathbf{r}'dt' + \int_{V,t}\mathbf{g}_{22}(\mathbf{r},t|\mathbf{r}',t')\cdot\mathbf{m}(\mathbf{r}',t')d\mathbf{r}'dt' \tag{4}$$

where (V, t) indicates the space-time domain over which the sources act.

Consider a GPR survey in which an EM source such as an electric dipole is energized with a source waveform $S(t)$, and the transient electric field is measured at positions $\mathbf{r}_i$ (i = 1, 2,…, NR) from time $t = 0$ to $t = T$. Let $\mathbf{e}_0(\mathbf{r}_i, t)$ denote these measurements and assume all fields are zero for $t < 0$. The goal of GPR inversion is to find a model [a conductivity distribution $\sigma(\mathbf{r}')$ and/or a permittivity distribution $\varepsilon(\mathbf{r}')$] such that the transient electric field $\mathbf{e}(\mathbf{r}_i, t)$ calculated for the model fits the observed field in some sense. Here we denote $\mathbf{r}'$ as a point in the domain over which the model is allowed to vary and $\mathbf{r}$ denotes a point in the region where measurements are made. An obvious choice is to match the data in a least-squares sense, which corresponds to finding a model that minimizes the error functional

$$R_d(\mathbf{p}) = \frac{1}{2}\sum_{i=1}^{NR}\int_0^T[\mathbf{e}_0(\mathbf{r}_0,t)-\mathbf{e}(\mathbf{r}_t,t)]^2dt = \frac{1}{2}\sum_{i=1}^{NR}\int_0^T\delta\mathbf{e}_0(\mathbf{r}_t,t)\cdot\delta\mathbf{e}_0(\mathbf{r}_t,t)dt \tag{5}$$

where

$$\delta\mathbf{e}_0(\mathbf{r}_i,\ t) = \mathbf{e}_0(\mathbf{r}_i,\ t)-\mathbf{e}(\mathbf{r}_i,\ t) \tag{6}$$

indicates the difference between the observed and predicted electric fields. The dependence of the error functional R_d on the model comes from the implicit dependence of the calculated model response **e** on model parameters **p** (σ and ε).

The most straightforward way of minimizing the non-linear functional R_d is the gradient or steepest descent algorithm. Let γ denote the gradient of R_d with respect to **p**, i.e.,

$$\gamma = \delta R_d/\delta\mathbf{p},\ (\gamma_s = \delta R_d/\delta\sigma,\ \text{and/or}\ \gamma_\varepsilon = \delta R_d/\delta\varepsilon). \tag{7}$$

In the steepest descent algorithm the model is updated by a step along the gradient direction as

$$\mathbf{p}^{(k+1)} = \mathbf{p}^{(k)}-\alpha^{(k)}\gamma^{(k)}, \tag{8}$$

where k indicates the iteration number, and α is the step length.

Taylor expansion of R_d around **p** is represented as

$$R_d(\mathbf{p}+\delta\mathbf{p}) = R_d(\mathbf{p})+\delta\mathbf{p}\frac{\partial}{\partial\mathbf{p}}R_d(\mathbf{p})+\frac{1}{2}\left(\delta\mathbf{p}\frac{\partial}{\partial\mathbf{p}}\right)^2R_d(\mathbf{p})+... \tag{9}$$

from which a small perturbation of R_d about the current model, δR_d, can be written as

$$\delta R_d \equiv R_d(\mathbf{p}+\delta\mathbf{p})-R_d(\mathbf{p}) = <\gamma,\delta\mathbf{p}> + O(\delta\mathbf{p}^2). \tag{10}$$

where

$$<\gamma,\delta\mathbf{p}> = \int_V\gamma(\mathbf{r}')\cdot\delta\mathbf{p}(\mathbf{r}')d\mathbf{r}', \tag{11}$$

indicates a linear functional and V' is the region where the model is allowed to vary.

When model parameters are changed to $\mathbf{p}' = \mathbf{p} + \delta\mathbf{p}$, EM fields vary to $\mathbf{e}' = \mathbf{e} + \delta\mathbf{e}$ and $\mathbf{h}' = \mathbf{h} + \delta\mathbf{h}$. Dropping terms involving the product of two perturbed quantities gives

$$\left(\sigma+\varepsilon\frac{\partial}{\partial t}\right)\delta\mathbf{e}-\nabla\times\delta\mathbf{h} = -\left(\delta\sigma+\delta\varepsilon\frac{\partial}{\partial t}\right)\mathbf{e}, \tag{12}$$

$$\nabla\times\delta\mathbf{e}+\mu\frac{\partial\delta\mathbf{h}}{\partial t} = 0, \tag{13}$$

The solution of these equations is given by

$$\delta\mathbf{e}(\mathbf{r}_i,t) = \int_0^t\int_{V'}\mathbf{g}_{11}(\mathbf{r},t|\mathbf{r}',t')\cdot\left[\delta\sigma(\mathbf{r}')+\delta\varepsilon(\mathbf{r}')\frac{\partial}{\partial t'}\right]\mathbf{e}(\mathbf{r}',t')d\mathbf{r}'dt'\ . \tag{14}$$

Furthermore, the error function can be rewritten as

$$R_d(\mathbf{p}+\delta\mathbf{p}) = \frac{1}{2}\sum_{i=1}^{NR}\int_0^T[\mathbf{e}_0(\mathbf{r}_t,t)-\mathbf{e}'(\mathbf{r}_t,t)]^2dt \tag{15}$$

From Eqs. (5), (10) and (15), we have

$$\delta R_d = \frac{1}{2}\sum_{i=1}^{NR}\int_0^T\{[\mathbf{e}_0(\mathbf{r}_i,t)-\mathbf{e}'(\mathbf{r}_i,t)]^2-[\mathbf{e}_0(\mathbf{r}_i,t)-\mathbf{e}(\mathbf{r}_i,t)]^2\}dt$$

$$= -\sum_{i=1}^{NR}\int_0^T\left[\delta\mathbf{e}_0(\mathbf{r}_i,t)\cdot\delta\mathbf{e}(\mathbf{r}_i,t)-\frac{1}{2}\delta\mathbf{e}(\mathbf{r}_i,t)\cdot\delta\mathbf{e}(\mathbf{r}_i,t)\right]dt$$

$$\approx -\sum_{i=1}^{NR}\int_0^T\delta\mathbf{e}_0(\mathbf{r}_i,t)\cdot\delta\mathbf{e}(\mathbf{r}_i,t)dt \tag{16}$$

Substituting equation (14) into equation (16) and using equations (7), (10) and (11), we obtain

$$\gamma_\sigma(\mathbf{r}') = -\sum_{i=1}^{NR}\int_0^T dt\,\delta\mathbf{e}_0(\mathbf{r},t)\cdot\int_0^t\mathbf{g}_{11}(\mathbf{r},t|\mathbf{r}',t')\cdot\mathbf{e}(\mathbf{r}',t')dt', \tag{17a}$$

$$\gamma_\varepsilon(\mathbf{r}') = -\sum_{i=1}^{NR}\int_0^T dt\,\delta\mathbf{e}_0(\mathbf{r},t)\cdot\int_0^t\mathbf{g}_{11}(\mathbf{r}_i,t|\mathbf{r}',t')\cdot\frac{\partial}{\partial t'}\mathbf{e}(\mathbf{r}',t')dt', \tag{17b}$$

The gradients γ_σ and γ_ε correspond to partial derivatives of the error functional R_d with respect to the conductivity σ and the permittivity ε at $\mathbf{r}'$. Thus, for example, equation (17a) indicates that γ_σ at $\mathbf{r}'$ is obtained by correlating the electric-field errors $\delta\mathbf{e}_0$ at all measurement points with the electric field $\mathbf{e}$ caused by a point electric current source at $\mathbf{r}'$ that has the same direction and the same time dependence as the electric field at $\mathbf{r}'$ in the current model. Equations (17a) and (17b) require one forward modeling to compute the fields in the current model and as many more forward modelings as there are image points to compute the gradients. This quickly becomes impractical as the number of imaging points becomes large.

Reversing the order of integration over t and t', and taking care to cover the same integration domain yield

$$\gamma_\sigma(\mathbf{r}') = -\sum_{i=1}^{NR}\int_0^T dt'\int_{t'}^T dt\,\delta\mathbf{e}_0(\mathbf{r},t)\cdot\mathbf{g}_{11}(\mathbf{r},t|\mathbf{r}',t')\cdot\mathbf{e}(\mathbf{r}',t'), \tag{18a}$$

$$\gamma_\varepsilon(\mathbf{r}') = -\sum_{i=1}^{NR}\int_0^T dt'\cdot\int_{t'}^T dt\,\delta\mathbf{e}_0(\mathbf{r},t)\cdot\mathbf{g}_{11}(\mathbf{r}_i,t|\mathbf{r}',t')\cdot\frac{\partial}{\partial t'}\mathbf{e}(\mathbf{r}',t'). \tag{18b}$$

From the reciprocity relation of equation (A7), we have

$$\gamma_\sigma(\mathbf{r}') = \int_0^T dt'\,\mathbf{e}(\mathbf{r}',t')\cdot\mathbf{e}_b(\mathbf{r}',t'|\delta\mathbf{e}_0), \tag{19a}$$

$$\gamma_\varepsilon(\mathbf{r}') = \int_0^T dt'\frac{\partial}{\partial t'}\mathbf{e}(\mathbf{r}',t')\cdot\mathbf{e}_b(\mathbf{r}',t'|\delta\mathbf{e}_0), \tag{19b}$$

where

$$\mathbf{e}_b(\mathbf{r}',t'|\delta\mathbf{e}_0) = \sum_{i=1}^{NR}\int_T^{t'} dt\,\mathbf{g}_{11}^{+}(\mathbf{r}',t'|\mathbf{r}_i,t)\cdot\delta\mathbf{e}_0(\mathbf{r}_i,t) \tag{20}$$

is the back-propagated field starting from $t = T$. The adjoint Green dyadic $\mathbf{g}_{11}^{+}$ (see Appendix A) gives the electric field at $\mathbf{r}'$ and t' caused by an electric current source $\delta\mathbf{e}_0$ radiating at $\mathbf{r}_i$ at a later time t. The reversal of the time order is implicit in the definition of the adjoint Green dyadics, because they are anti-causal. From equation (19), we can find that the gradient γ can also be obtained by correlating the actual electric field $\mathbf{e}$ at $\mathbf{r}'$ with the back-propagated electric field $\mathbf{e}_b$.

3. INVERSION PROCEDURE

Although equation (19) is simply rewritten from equation (17) using the definition of the adjoint Green dyadics, we have a great advantage in computing the gradients with the new equations. The properties of the adjoint dyadic $\mathbf{g}_{11}^{+}$ imply that the back-propagated field $\mathbf{e}_b$ satisfy equations adjoint to the Maxwell's equations and that the source terms for these adjoint equations are the data error $\delta\mathbf{e}_0$ at all receivers radiating as electric current sources in reverse time, i.e.,

$$\left(\varepsilon\frac{\partial}{\partial t}+\sigma\right)\mathbf{e}_b+\nabla\times\mathbf{h}_b = -\sum_i\delta\mathbf{e}_0(\mathbf{r}_i,t)\delta(\mathbf{r}-\mathbf{r}_i), \tag{21}$$

$$-\nabla\times\mathbf{e}_b-\mu\frac{\partial\mathbf{h}_b}{\partial t} = 0. \tag{22}$$

These equations follow directly from equations (A8) and (A9). The back-propagated fields can thus be obtained by stepping these equations backward in time from $t = T$ with, for example, a finite difference time-domain (FDTD) algorithm (see Appendix B). Although Maxwell's equations (1) and (2) are unstable when stepped backward in time, adjoint equations (21) and (22) are stable. In fact, these equations can be stepped backward in time with the same FDTD algorithm that marches the ordinary Maxwell's equations forward in time (see Appendix B). Consequently, the quantities needed to compute the gradients can be obtained with just two modelings: one is forward modeling with the Maxwell's equations ($\mathbf{m} = 0$ assumed) to compute the fields in the current model, and the other reverse modeling with the adjoint equations to compute the back-propagated fields.

Extension of this derivation for a multiple-source problem is trivial. All fields contain an additional argument to represent their dependence on source positions $\mathbf{s}_j$ ($j = 1, 2,\ldots, NS$), and thus the error functional R_d requires an additional summation over index j,

$$R_d(\mathbf{p}) = \frac{1}{2}\sum_{j=1}^{NR}\sum_{i=1}^{NR}\int_0^T[\mathbf{e}_0(\mathbf{r}_i,t;\,\mathbf{s}_j)-\mathbf{e}(\mathbf{r}_i,t;\,\mathbf{s}_j)]^2dt \tag{23}$$

The gradients for full set of data from all source positions are just the sum of the gradients from each source position independently,

$$\gamma_\sigma(\mathbf{r}') = \sum_{j=1}^{NS}\int_0^T dt'\mathbf{e}(\mathbf{r}',t';\mathbf{s}_j)\cdot\mathbf{e}_b(\mathbf{r}',t'|\delta\mathbf{e}_0(\mathbf{s}_j)), \quad (24a)$$

$$\gamma_\varepsilon(\mathbf{r}') = \sum_{j=1}^{NS}\int_0^T dt'\frac{\partial}{\partial t'}\mathbf{e}(\mathbf{r}',t';\mathbf{s}_j)\cdot\mathbf{e}_b(\mathbf{r}',t'|\delta\mathbf{e}_0(\mathbf{s}_j)), \quad (24b)$$

Computation of the modeled data and the gradients now requires one forward and reverse modeling for each source position.

To implement the above equations, we must of course discretize both the model and data. A staggered grid (Yee, 1966) is useful for stable computation even on a place where conductivity steeply varies. We have mentioned above that the same FDTD algorithm can be used for both forward modeling and back-propagation, and that the stability properties of these two operations are similar. However, in the full-waveform inversion, a large amount of computer memory is needed because evaluating the gradients requires the full set of wavefields from all source positions. Sanada et al. (1999b) computed the spatial derivatives by using the Fourier pseudo-spectral method (e.g., Carcione, 1996), from which the required grid spacing may be increased to reduce computer memory.

The steepest descent method described above usually converges very slowly near a minimum of the error functional R_d (Press et al., 1992). A better approach can be the CG method, which updates the current model $\mathbf{p}^{(k)}$ by moving along a search direction determined by the gradient of R_d and the previous search direction as

$$\mathbf{p}^{(k+1)} = \mathbf{p}^{(k)} + \alpha^{(k)}b^{(k)}. \quad (25)$$

where $\alpha^{(k)}$ is the step length and

$$b^{(k)} = -\gamma^{(k)} + \beta^{(k)}b^{(k-1)}, \quad (26)$$

is the search direction. The scalar parameter $\beta^{(k)}$ can be updated the Polak-Ribiere choice (Press et al., 1992):

$$\beta^{(k)} = \frac{\langle\gamma^{(k)},\gamma^{(k)}-\gamma^{(k-1)}\rangle}{\langle\gamma^{(k-1)},\gamma^{(k-1)}\rangle} \quad (27)$$

The search direction is reset to the steepest descent direction if $\beta^{(k)} = 0$. The step length $\alpha^{(k)}$ can be determined by simple searches such as the Brent's method (Press et al., 1992).

Finally, for judging the convergence of the inversion, we define normalized (rms) data error E as

$$E = \sqrt{\sum_{j=1}^{NS}\sum_{i=1}^{NR}\int_0^T(\mathbf{e}_0-\mathbf{e})^2dt}\Bigg/\sqrt{\sum_{j=1}^{NS}\sum_{i=1}^{NR}\int_0^T\mathbf{e}_0^2dt} \quad (28)$$

The process of the inversion is summarized:

1) Construct a proper initial model.
2) Compute its electric fields $\mathbf{e}(\mathbf{r}', t'; \mathbf{s}_j)$ through FDTD modeling.
3) Calculate $\mathbf{e}_b(\mathbf{r}',t'|\delta\mathbf{e}_0(\mathbf{s}_j))$ by back-propagating the electric field difference $\delta\mathbf{e}_0(\mathbf{r}_i, t; \mathbf{s}_j)$ with the adjoint dyadic $\mathbf{g}_{11}^{+}$.
4) Update the current model with $\gamma(\mathbf{r}')$ obtained from the cross-correlation of $\mathbf{e}(\mathbf{r}', t'; \mathbf{s}_j)$ and $\mathbf{e}_b(\mathbf{r}',t'|\delta\mathbf{e}_0(\mathbf{s}_j))$.
5) Repeat the process 2) – 4) until convergence.

4. NUMERICAL VERIFICATION

Figure 1 shows a two-dimensional (2-D) model for validating the full waveform inversion algorithm described above. This model consists of two 50 cm × 50 cm anomalous bodies in a uniform whole space whose dielectric constant is 4. The bodies have dielectric constants of 9 and 2, respectively. For simplicity, the model is assumed to be constant conductivity of 1 mS/m. A crosshole configuration is used for the exercise; a total of 21 sources with an equal vertical separation of 50 cm, while a total of 101 receivers with an equal distance of 10 cm. The horizontal distance between source and receiver at a same depth is 5 m. A grid consisting of 150 × 100 elements of uniform cell size, 10 cm × 10 cm, is used to compute EM wavefields in transverse magnetic mode using a FDTD modeling scheme with the perfectly matched layer. For each source, a Ricker wavelet with a dominant frequency of 100 MHz is added. The explicit time marching is stable when Δt = 0.16 ns in the FDTD

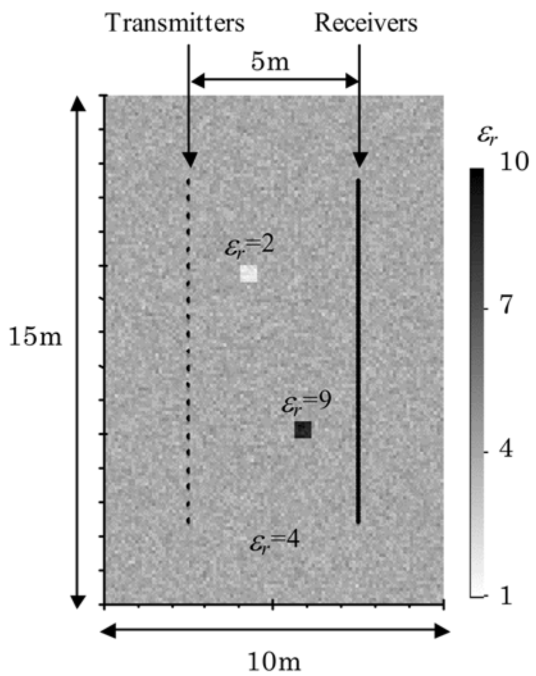

Fig. 1. A synthetic model for numerical simulation of crosshole radar imaging; 21 sources and 101 receivers are distributed at the left and right boreholes, respectively.

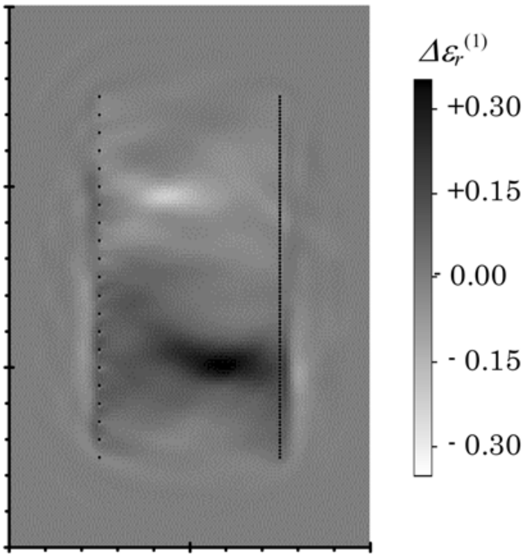

Fig. 2. Relative permittivity updates at the first inversion step, $\Delta\varepsilon_r^{(1)}$, suggesting a correct model updating is made in the inversion.

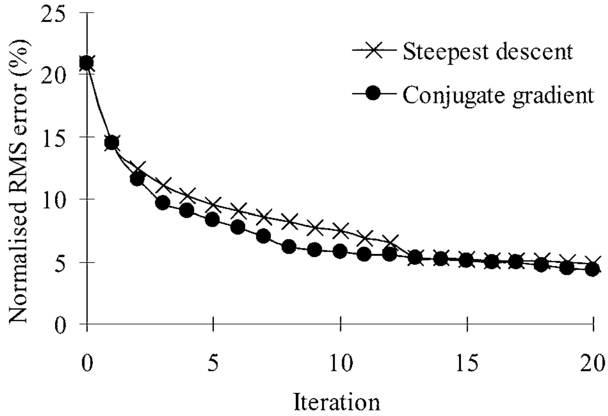

Fig. 4. Convergence of normalized data misfits as a function of iteration during the full-waveform inversion.

scheme. The synthetic data generated for the model shown in Figure 1 are contaminated with 10 % Gaussian noise.

An inversion experiment is made using a homogeneous whole-space of $\varepsilon_r = 4$ as an initial model. An optimum step length $\alpha^{(k)}$ is determined by the Brent's method which requires 7 – 9 forward calculations at each iteration. Figure 2 shows relative permittivity updates at the first inversion step, $\Delta\varepsilon_r^{(1)}$, which are evaluated from the correlations between forward wavefields and back-propagated residual wavefields. This result clearly shows that correct model updating will be made in the inversion. Our inversion is terminated after 20 iterations to produce a relative permittivity section shown in Figure 3. Total computing time was about 5 hours on 2.93 GHz PC with 512 MB memory. The images show much sharper resolution in the vertical direction than in the horizontal direction as usual in crosshole surveys. The inversion process is quite stable as shown in Figure 4; the normalized data error (28) decreases from more than 21 % to less than 6 % after 8th iteration in the CG method, and subsequent iterations show a slow decrease of the error. As expected, the CG search is more efficient to reduce the misfit functional than the steepest descent technique as shown in Figure 4.

5. CONCLUSIONS

The cross correlation of back-propagated upcoming waves with the downward traveling incident waves is used for wave equation migration of seismic data (Claerbout, 1971). Tarantola (1984) showed later that these operations were the same as moving down the gradient of least-squares functional and thereby tied together seismic migration with a single step of nonlinear inversion by a gradient search. This formalism for wavefield imaging or inversion carries over directly to EM fields governed by the Maxwell's equations. The only difference is that the wave equation is self-adjoint so that the equations for the forward and backward propagation of wavefields are the same, whereas those of the EM fields are different: Maxwell's equations and their adjoint equations (Appendix A). This difference, however,

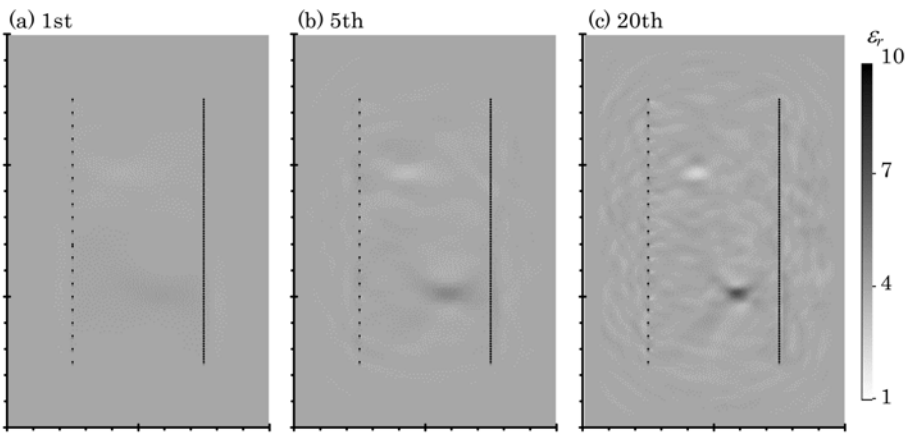

Fig. 3. Relative permittivity images obtained after (a) 1st, (b) 5th, and (c) 20th inversion iteration.

is rather formal, because the same modeling code that marches the original equations forward in time can march the adjoint equations backward in time. In the computation of gradients, however, the forward-propagated fields are stored at all sampled time points employed in the FDTD scheme. Such field sampling significantly increases the memory needed for storing the forward-propagated fields.

The inversion algorithm has been verified using a 2D model having non-uniform permittivity distribution. Tests on the synthetic model simulating crosshole radar surveys produced good images of two block scatterers and showed stable convergence. The CG technique is more efficient to reduce the misfit functional than the steepest descent search. For faster and more stable convergence we may utilize several techniques: weightings of error functional and model parameters, regularization of the problem, smoothing filter, etc. Extending of the proposed algorithm to 3D problems with applications to real data requires further investigation.

ACKNOWLEDGMENTS: This work was supported by Pukyong National University Research Foundation Grant in 2005 (PR-2005-018) and the KOSEF-JSPS Cooperative Program (F01-2006-000-10248-0).

REFERENCES

Carcione, J. M., 1996, Ground-penetrating radar: Wave theory and numerical simulation in lossy anisotropic media. Geophysics, 61, 1664–1677.

Claerbout, J. F., 1971, Toward a unified theory of reflector mapping. Geophysics, 36, 467–481.

Ha, T., Min, D.-J., Shin, C., and Pyun, S., 2004, Electric resistivity inversion via reverse time migration algorithm of seismic data. 74th Ann. Internat. Mtg., Soc. Expl. Geophys., Expanded Abstracts.

Jia, H., Takenaka, T., and Tanaka, T., 2002, Time-domain inverse scattering method for cross-borehole radar imaging. IEEE Trans. Geosci. Remote Sensing, GR-40, 1640–1647.

Newman, G. A., and Commer, M., 2005, New advances in three dimensional transient electromagnetic inversion. Geophys. J. Int., 160, 5–32.

Press, W. H., Teukolsky, S. A., Vetterling, W. T., and Flannery, B. P., 1992, Numerical Recipes in Fortran: The Art of Scientific Computing: Cambridge Univ. Press.

Sanada, Y., Matsuoka, T., Yamamoto, K., Watanabe, T., and Ashida, Y., 1999a, Inversion of EM tomography by gradient method. Proc. 100th SEGJ Conf., 173–176. (in Japanese)

Sanada, Y., Matsuoka, T., and Ashida, Y., 1999b, EM wave modeling by finite difference time domain method using Pseudo spectral method. Proc. 100th SEGJ Conf., 232–235. (in Japanese with English abstract)

Tai, C. T., 1993, Dyadic Green Functions in Electromagnetic Theory, 2nd ed. IEEE Press.

Tarantola, A., 1984, Inversion of seismic reflection data in the acoustic approximation. Geophysics, 49, 1259–1266.

Wang, T., Oristaglio, M., Tripp, A., and Hohmann, G., 1994, Inversion of diffusive transient electromagnetic data by a conjugate-gradient method. Radio Science, 29, 1143–1156.

Yee, K.S., 1966, Numerical solution of initial boundary problems involving Maxwell's equations in isotropic media. IEEE Trans. Ant. Prop., AP-14, 302–309.

APPENDIX A. GREEN FUNCTION

The four Green dyadics in equations (3) and (4) satisfy the following first-order equations:

$$\left(\sigma+\varepsilon\frac{\partial}{\partial t}\right)\mathbf{g}_{11}-\nabla\times\mathbf{g}_{21} = -\mathbf{i}\delta(\mathbf{r}-\mathbf{r}')\delta(t-t'), \tag{A1}$$

$$\nabla\times\mathbf{g}_{11}+\mu\frac{\partial\mathbf{g}_{21}}{\partial t} = 0, \tag{A2}$$

$$\left(\sigma+\varepsilon\frac{\partial}{\partial t}\right)\mathbf{g}_{12}-\nabla\times\mathbf{g}_{22} = 0, \tag{A3}$$

$$\nabla\times\mathbf{g}_{12}+\mu\frac{\partial\mathbf{g}_{22}}{\partial t} = -\mathbf{i}\delta(\mathbf{r}-\mathbf{r}')\delta(t-t'), \tag{A4}$$

and are causal,

$$\mathbf{g}_{ij}(\mathbf{r},\ t|\mathbf{r}',\ t') \equiv 0, \qquad t\le t', \tag{A5}$$

where $\mathbf{i}$ is the identity tensor. The adjoint Green dyadics, $\mathbf{g}^+$, are defined by

$$\mathbf{g}^+_{ij}(\mathbf{r}',t'|\mathbf{r},t)\equiv\tilde{\mathbf{g}}_{ij}(\mathbf{r},t|\mathbf{r}',t'), \tag{A6}$$

where ~ indicates the transpose of dyadic, e.g.,

$$\hat{\mathbf{x}}\cdot\mathbf{g}\cdot\hat{\mathbf{z}} = \hat{\mathbf{z}}\cdot\tilde{\mathbf{g}}\cdot\hat{\mathbf{x}}. \tag{A7}$$

where ^ denotes the unit vector. In other words, equation (A6) represents the reciprocity relation for transient EM fields. The adjoint Green dyadics satisfy the following equations (obtained from equations (A1) – (A4) by reversing the sign of all space-time coordinates):

$$\left(\sigma-\varepsilon\frac{\partial}{\partial t}\right)\mathbf{g}^+_{11}+\nabla\times\mathbf{g}^+_{21} = -\mathbf{i}\delta(\mathbf{r}-\mathbf{r}')\delta(t-t'), \tag{A8}$$

$$-\nabla\times\mathbf{g}^+_{11}-\mu\frac{\partial\mathbf{g}^+_{21}}{\partial t} = 0, \tag{A9}$$

$$\left(\sigma-\varepsilon\frac{\partial}{\partial t}\right)\mathbf{g}^+_{12}+\nabla\times\mathbf{g}^+_{22} = 0, \tag{A10}$$

$$-\nabla\times\mathbf{g}^+_{12}-\mu\frac{\partial\mathbf{g}^+_{22}}{\partial t} = -\mathbf{i}\delta(\mathbf{r}-\mathbf{r}')\delta(t-t'), \tag{A11}$$

and are anticausal,

$$\mathbf{g}^+_{ij}(\mathbf{r},\ t|\mathbf{r}',\ t') \equiv 0, \qquad t\ge t'. \tag{A12}$$

APPENDIX B. STABILITY OF FDTD SCHEMES

Forward modeling and back-propagation are done with a finite-difference time-domain (FDTD) method. In this appendix we consider the stability properties of these two operations. For simplicity, we restrict our discussion to a 2D model with line sources and assume that displacement currents can be neglected. The Maxwell's equations are then reduced to a scalar diffusion equation as

$$\nabla^2 e - \mu\sigma\frac{\partial e}{\partial t} = -s(x, z, t)\,, \tag{B1}$$

where $s(x, z, t)$ represents a general source term. Let

$$e^k_{m,n} = e(x_m, z_n, t_k)\,,$$

be the electric field at time $t_k = k\Delta t$ on a regular 2D grid with a grid spacing h. A simple algorithm for marching equation (B1) forward in time replaces the Laplacian with a five-point difference approximation and uses a forward difference for the time derivative as

$$\nabla^2 e(x_m, z_n, t_k) \approx \frac{1}{h^2}(e^k_{m+1,n} + e^k_{m-1,n} + e^k_{m,n+1} + e^k_{m,n-1} - e^k_{m,n}),$$

and

$$\frac{\partial e}{\partial t} \approx \frac{1}{\Delta t}(e^{k+1}_{m,n} - e^k_{m,n})\,.$$

These produce a time-stepping scheme

$$e^{k+1}_{m,n} = (1-4\alpha)e^k_{m,n} + \alpha(e^k_{m+1,n} + e^k_{m-1,n} + e^k_{m,n+1} + e^k_{m,n-1} - e^k_{m,n})\,. \tag{B2}$$

where $\alpha = \Delta t / (\sigma\mu h^2)$. Starting from fields at $t = 0$ (usually $e^0 \equiv 0$), equation (B2) can be used to advance fields at all grid points to the next time $t = \Delta t$. A standard result is that this explicit time marching is stable if $\alpha \le 1/4$. We refer to this type of approximation as DF.

Next we derive finite difference approximations of equation (B1) for reverse time marching. The backward difference approximation to the time derivative is

$$\frac{\partial e}{\partial t} \approx \frac{1}{\Delta t}(e^k_{m,n} - e^{k-1}_{m,n})\,,$$

and the finite difference approximation is

$$e^{k-1}_{m,n} = (1+4\alpha)e^k_{m,n} - \alpha(e^k_{m+1,n} + e^k_{m-1,n} + e^k_{m,n+1} + e^k_{m,n-1} + h^2 s^k_{m,n})\,. \tag{B3}$$

The diffusion equation describes fields that are decaying in forward time but growing in reverse time. It is why the diffusion equation is unstable when marched backward in time. We refer to this type of approximation as DB.

In the adjoint equation (concentration equation), the sign of the time derivative term in equation (B1) is reversed to produce

$$\nabla^2 e + \mu\sigma\frac{\partial e}{\partial t} = -s(x, z, t)\,. \tag{B4}$$

Using the forward difference approximation to the time derivative, we have

$$e^{k+1}_{m,n} = (1+4\alpha)e^k_{m,n} - \alpha(e^k_{m+1,n} + e^k_{m-1,n} + e^k_{m,n+1} + e^k_{m,n-1} + h^2 s^k_{m,n})\,. \tag{B5}$$

This equation is the same as equation (B3) except for different time indices on the left-hand side, and therefore unstable (refer to as AF). Finally, the difference approximation of the adjoint equation backward in time is given by

$$e^{k-1}_{m,n} = (1-4\alpha)e^k_{m,n} + \alpha(e^k_{m+1,n} + e^k_{m-1,n} + e^k_{m,n+1} + e^k_{m,n-1} + h^2 s^k_{m,n})\,. \tag{B6}$$

This is the same as DF except for the time index, and therefore stable (refer to as AB).

In summary,

1) DF is used for the calculation forward in time.
2) DB is used for the calculation backward in time.
3) AF has the same finite difference approximation as DB, and both are unstable.
4) AB has the same finite difference approximation as DF, and both are stable.

In the full-waveform inversion described above, we use DF and AB for the forward and backward time continuations, respectively, and these are the same and therefore stable.

Manuscript received October 20, 2006
Manuscript accepted August 27, 2007